Co-existence of ferroelectricity and ferromagnetism in 1.4 nm $SrBi_2Ta_2O_{11}$ film

2003 J. Phys.: Condens. Matter 15 7901

(http://iopscience.iop.org/0953-8984/15/46/009)

INSTITUTE OF PHYSICS PUBLISHING JOURNAL OF PHYSICS: CONDENSED MATTER

J. Phys.: Condens. Matter **15** (2003) 7901–7915 PII: S0953-8984(03)66681-6

Co-existence of ferroelectricity and ferromagnetism in 1.4 nm $SrBi_2Ta_2O_{11}$ film

M-H Tsai[1], Y-H Tang[1] and Sandwip K Dey[2]

[1] Department of Physics, National Sun Yat-Sen University, Kaohsiung 804, Taiwan
[2] Department of Chemical and Materials Engineering and Electrical Engineering, Arizona State University, Tempe, AZ 85287-6006, USA

Received 24 July 2003, in final form 10 October 2003
Published 7 November 2003
Online at stacks.iop.org/JPhysCM/15/7901

Abstract

In pseudo-tetragonal strontium bismuth tantalate, $SrBi_2Ta_2O_9$ (SBT), with two formula units per unit cell, bismuth oxide $\{(Bi_2O_2)^{2+}\}$ layers alternate with double strontium tantalate perovskite layers $\{(SrTa_2O_7)^{2-}\}$. A unit cell of SBT is truncated to form a sub-cell or film, of composition $SrBi_2Ta_2O_{11}$, which is 1.4 nm thick and comprised of a bottom $(BiO_2)^{1+}$ layer, a central $(SrTa_2O_7)^{2-}$ layer and a top $(BiO_2)^{1+}$ layer. Using spin-polarized first-principles calculations, it is found that this $SrBi_2Ta_2O_{11}$ film is multi-ferroic, magnetoelectric, i.e. it simultaneously exhibits ferroelectric and ferromagnetic characteristics. When Ta ions are collectively displaced in the *ab* plane and in the [110] direction, the calculated double potential energy well, with a depth of −3.1 eV/unit cell at a Ta off-centre displacement of 0.032 nm, reflects the ferroelectric character. The calculated spin-polarized electronic structure reveals that ferromagnetism stems, not from the d electrons of the Ta ions, but predominantly from the unpaired p electrons of the O ions. The O ions in the Sr–O layer have the largest magnetic moment of 1.32 μ_B. Specifically, the ferromagnetic character is mediated by the unoccupied states of the Sr 5p band above the Fermi level, E_F. These states provide a mechanism for the double exchange or hopping of highly localized O 2p (majority) spins between adjacent O ions located on both sides of the Sr ion.

(Some figures in this article are in colour only in the electronic version)

1. Introduction

Layered perovskite (Aurivillius) oxides such as multi-component strontium bismuth tantalate ($SrBi_2Ta_2O_9$ or SBT), with two formula units per unit cell, are of technological importance owing to their switchable spontaneous polarization or ferroelectric behaviour, high dielectric permittivity and piezoelectric or pyroelectric properties [1–9]. Currently, SBT films are being considered for nonvolatile, random-access memories [10]. In pseudo-tetragonal structured

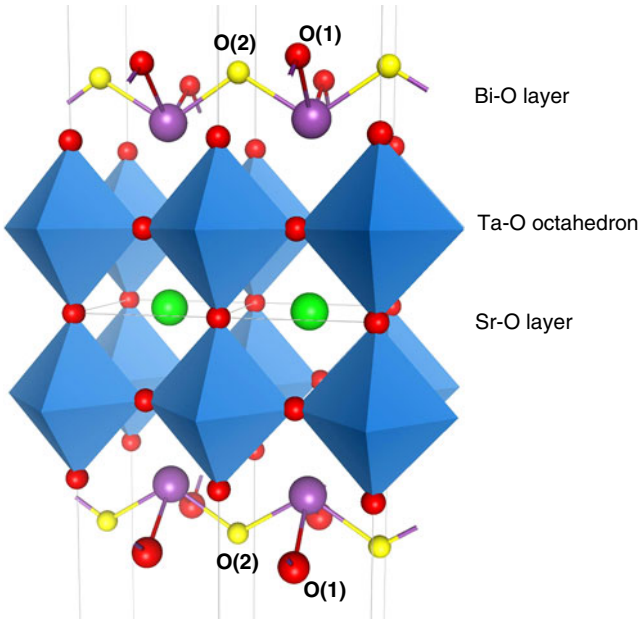

Figure 1. A side view of the $SrBi_2Ta_2O_{11}$ film.

SBT, the sublattices in the direction of the *c* axis are comprised of alternating bismuth oxide $\{(Bi_2O_2)^{2+}\}$ and double strontium tantalate $\{(SrTa_2O_7)^{2-}\}$ perovskite layers of oxygen octahedra. The dual crystal chemistries [3, 4] gives rise to dual electronic and dielectric properties that are unique to such Aurivillius phases.

Due to the current interest in nanoscience and nanotechnology, there is a critical need to design and fabricate novel multifunctional materials at the nanoscale. Since conventional SBT contains a Sr ion (with localized 2p states above the Fermi level, E_F [11]), Bi ions (with a $6s^2$ lone pair) and octahedral Ta ions (with 5d electrons), in nanometre dimensions it may exhibit unique multi-ferroic properties such as magnetoelectricity. Therefore, the central theme of this paper is to determine the electronic and potentially unique properties of SBT-derived films that are nanometres (nm) thick.

If a unit cell of conventional SBT is truncated to form a nm-thick sub-cell, it will be comprised of a bottom $(BiO_2)^{1+}$ layer, a central $(SrTa_2O_7)^{2-}$ layer and a top $(BiO_2)^{1+}$ layer. Figure 1 illustrates this sub-cell (of SBT) or film with oxygen-rich surfaces, which is 1.4 nm thick and has a composition of $SrBi_2Ta_2O_{11}$. Note the $SrBi_2Ta_2O_{11}$ composition is equivalent to the replacement of Bi_2O_3 with Bi_2O_5 in SBT. This is plausible because Bi can exist in both Bi^{3+} and Bi^{5+} oxidation states [12].

Using spin-polarized first-principles calculations, it is found that nm-thick $SrBi_2Ta_2O_{11}$ films are magnetoelectric, i.e. they simultaneously exhibit ferroelectric and ferromagnetic characteristics. The physical origin of this phenomenon is discussed in the light of the

(a) collective off-centre displacement of Ta in the *ab* plane and in the [110] direction,
(b) O-rich composition that enables the existence of non-bonded and highly localized O 2p electrons having a net spin, and
(c) presence of localized Sr 5p states above the energy, E_F, that mediate ferromagnetic coupling among spins.

2. Background

This section briefly describes the (a) understanding of the magnetoelectric effect to date, (b) previous results of first-principles calculations of the electronic structure of conventional SBT, (c) first-principles calculations of the total energy in conventional SBT and (d) the scalability issue in thin-film ferroelectrics.

2.1. Potential origin of the magnetoelectric effect

It has been known that certain multi-component oxides are multi-ferroic, magnetoelectric materials. Magnetoelectric materials simultaneously exhibit ferroelectric and ferromagnetic characteristics, i.e. their spontaneous polarization and spontaneous magnetization can be switched by applied electric and applied magnetic fields, respectively. Since lattice distortions are involved in insulators and/or semiconductor ferroelectrics, whereas a spin coupling among d electrons occurs in metallic or semi-metallic ferromagnetic materials, their simultaneous existence is rare. Although only a few are known to exist in nature, e.g. ferroelectric $BaMnF_4$ is found to be weakly ferromagnetic [13, 14], recent experimental and theoretical analyses have shown that multi-component monoclinic bismuth manganite, $BiMnO_3$ [15–17], hexagonal yttrium manganite, $YMnO_3$ [18, 19], and tetragonal bismuth ferrite, $BiFeO_3$ [20], are magnetoelectric materials [21].

Based on first-principles calculations, Hill [22] concluded that the scarcity of natural magnetoelectric materials is due to the simultaneous requirements of zero and non-zero occupancy of d orbitals in octahedral B-site cations for the existence of ferroelectricity and ferromagnetism, respectively. However, in $BiMnO_3$ [15, 17, 22], while the occupancy of d orbitals of the Mn ion is responsible for ferromagnetism, the $6s^2$ lone pair of the Bi ion apparently drives the system towards the ferroelectric state.

Note the conventional thought for the existence of ferromagnetism in multi-component oxides is the presence of non-bonded and localized d (or f) electrons (of the cation), which gives rise to a net spin. The coupling among such spins manifests as magnetic properties. One can also argue that, in a given multi-component oxide system, if the dimensions are greatly reduced to the order of nanometres, non-d electrons of anions or cations could become highly localized, as observed in nanoparticles and molecules. This localization may give rise to coupling among spins, which could potentially lead to the observance of magnetic properties.

2.2. First-principles calculations of the electronic structure of SBT

Earlier tight-binding calculations of Robertson *et al* [23] and Robertson and Chen [24] indicated that SBT is an insulator (bandgap, $E_g \sim 5.1$ and 4.2 eV, respectively). Recently, Stachiotti *et al* [25] and Peacock and Robertson [26] used plane-wave-based first-principles calculations to obtain E_g of $\sim$2 eV and 1.7 eV, respectively. However, the unoccupied O 2p partial densities of states (PDOS) from all these calculations disagree with the near-edge x-ray absorption fine structure (NEXAFS) measurements of Hartmann *et al* [27, 28], which show a very sharp threshold in the O K-edge NEXAFS spectrum; note that the NEXAFS spectrum is inexplicably shifted by 5.1 eV. In contrast, the O 2p PDOS by Tsai and Dey [11], calculated using the first-principles pseudofunction method, agree well with the O K-edge NEXAFS spectrum of Hartmann *et al* [27]. Tsai and Dey [11] explained the sharp O K-edge NEXAFS threshold by the cut-off of the O 2p band at E_F; the existence of the O 2p band near E_F was due to hybridization with Sr 5p orbitals.

Although Hartmann *et al* [27] observed two lower energy features located at 2.3 and 3.4 eV in the ultraviolet–visible (UV–vis) absorption measurements, they concluded that

SBT has an energy gap of 4.2 eV. Tsai and Dey [11] explained the low energy features in the UV–vis absorption data of Hartmann *et al* as transitions between occupied Bi-6s to unoccupied Bi-6p states (i.e. 3.4 eV) and occupied Sr-5s to unoccupied Sr-5p states (i.e. 2.3 eV). Since the calculated partial and total DOS of Tsai and Dey [11] accounted for the observed photoemission, and x-ray and UV–vis absorption data [27, 28], the interpretation of Hartmann *et al* was not conclusive proof of the existence of E_g.

2.3. First-principles calculations of the total energy in SBT

Stachiotti *et al* [25] also studied the onset of ferroelectricity in SBT. Their approach was based on the small-vibration phonon frequency and eigenvector calculations of the undistorted, tetragonal structure. In their results, they observed an unstable mode comprised of (i) a large displacement of the TaO_6 perovskite-like block, relative to Bi, and perpendicular to the *c* axis, and (ii) a displacement of the octahedral Ta ion relative to its surrounding O ions. The eigenvector of the mode indicated that the lattice instability primarily arises from the attractive interaction between the Bi ion and the apex O ion of the Ta octahedron [25]. The calculated total energy as a function of the Bi displacement in the [110] direction, corresponding to the unstable mode, exhibited a potential well depth of 6 mRyd/cell at a Bi displacement (relative to the apex O ion) of 0.05 nm [25]. Note that an energy gain of 6 mRyd/primitive cell, with 14 atoms/cell, approximately corresponds to an average energy gain of 6 meV/atom. Since this is significantly lower than the thermal excitation energy (25 meV) at room temperature, Stachiotti *et al*'s conclusion that ferroelectricity in SBT is due to the large displacement of Bi ions with respect to the rest of the lattice is questionable. Moreover, Stachiotti *et al* did not consider the idea that, once the Bi moves away from its high-symmetry position, the local symmetry and small-vibration eigenmodes are no longer the same. Since SBT contains ions with large effective charges and large long-range electrostatic interactions, the changes in the small-vibration eigenmodes are particularly important for the stability of its ferroelectric phase. In contrast, Tsai and Dey [11] determined that the spontaneous polarization in SBT was due to the collective off-centre displacement of Ta ions. They calculated an energy gain of 0.26 eV/primitive cell for a Ta displacement of 0.015 nm in the [110] direction. Note the polarization due to the Bi displacement is expected to be smaller because Bi, with its larger electronegativity compared to Ta, has a smaller positive effective charge. Additionally, since the long-range electrostatic (dipole–dipole) interaction energy is inversely proportional to the cube of the distance, the collective Ta off-centre displacement would again be favoured because the separation between two $(Bi_2O_2)^{2+}$ layers (which is 1.25 nm) is twice as large compared to the separation between the two Ta octahedral layers.

2.4. Scalability issue in thin-film ferroelectrics

Progress in ferroelectric thin-film technology over the past decade has been possible due to the advances in sub-micron thin-film fabrication processes and the control over their ferroelectric properties. However, in ultra-thin films ($<$50 nm), the properties deviate from those of the bulk and ferroelectricity is apparently suppressed. This phenomenon is commonly referred to in the literature as 'size effects'. It has been explained by depolarization field, stress, space charge at electrode/ferroelectric interfaces and nanostructure, including grain size, domain size and phase purity [29–38]. In this study, these issues will not be addressed due to the chosen set of boundary conditions given below. However, in nm-thick single-crystal films, the reduced number of available dipoles could alter the total dipole–dipole interaction energy and whether a nm-thick SBT-derived film retains its ferroelectric property is still questionable. Hence the

Table 1. Positions of the Sr, Bi, Ta and O ions in a $SrBi_2Ta_2O_{11}$ film. The x and y coordinates are in terms of the lattice constant, $a = 0.3895$ nm. The z coordinates are in terms of $c = 2.506$ nm, which is the lattice constant along the c axis in conventional SBT.

Atom	x	y	z
O(1)	0.500	0.000	0.250
O(2)	0.000	0.500	0.250
Bi	0.500	0.500	0.200
O	0.000	0.000	0.200
Ta	0.000	0.000	0.088
O	0.500	0.000	0.088
O	0.000	0.500	0.088
Sr	0.500	0.500	0.000
O	0.000	0.000	0.000
Ta	0.000	0.000	−0.088
O	0.500	0.000	−0.088
O	0.000	0.500	−0.088
O	0.000	0.000	−0.200
Bi	0.500	0.500	−0.200
O(1)	0.500	0.000	−0.250
O(2)	0.000	0.500	−0.250

electronic structure and total energy calculations are important and necessary to clarify the scalability issue under specific boundary conditions.

3. Calculation of electronic structure and the total energy of the $SrBi_2Ta_2O_{11}$

This section briefly outlines (a) the boundary conditions of the proposed $SrBi_2Ta_2O_{11}$ cell (figure 1), which will be called the $SrBi_2Ta_2O_{11}$ film from here onwards and (b) the calculation method used to evaluate its electronic structures and total energy. Note that, in order to determine the existence of ferroelectricity in this system, the distortion of the Ta octahedra was confined in the [110] direction in the ab plane.

3.1. Boundary conditions

The phase-pure and defect-free $SrBi_2Ta_2O_{11}$ film is 1.4 nm thick and infinitely extended in the ab plane. It is assumed that the charges from the discontinuity in the polarization at the lateral surfaces are completely compensated, i.e. the depolarization field is zero and the space-charge effect is a non-issue. Since the sub-cell is unconstrained and there are no grain boundaries, the boundary stress is zero.

The lattice constant, a, in the ab plane of a $SrBi_2Ta_2O_{11}$ film is the same as that of a conventional SBT unit cell, which is 0.3895 nm. The position coordinates of the 16 atoms are given in table 1, in which the z coordinate is perpendicular to the film and the atomic positions in the z direction are with respect to the lattice constant, c (2.506 nm), of the SBT unit cell.

In order to carry out the calculations, the Ta ion displacements are considered for two individual cases. In one, the Ta ions are displaced normal to the surface (the z direction) and in the other they are 45° off of the a axis in the ab plane, i.e. in the [110] direction. For a full set of independent cases, the [100] direction also needs to be considered. It is not considered here because it has been previously reported that SBT has a shallower potential energy well in the [100] direction [11]. For a given Ta displacement normal to the surface, the apex O ion positions are optimized in the z direction by minimization of the total energy. Similarly, for

a given Ta displacement in the [110] direction, the positions of the O ions in the *ab* plane are optimized in the x and y directions by minimization of the total energy. Relaxation of all O and Bi ions and surface reconstructions are not considered in this study. The central focus has only been on ion displacements, which by electrostatic arguments are most likely to give rise to ferroelectricity.

3.2. The calculation method and spin-polarized calculations

The spin-polarized first-principles calculation method used in this study is the pseudofunction (PSF) method [39], which uses the local-spin-density approximation (LSDA) of von Barth and Hedin [40]. In the current calculations, the simple $V_{\text{in,next}} = \alpha V_{\text{new}} + (1-\alpha)V_{\text{in}}$ mixing scheme was used for the self-consistent iterations. Here, V_{in} is the input potential used to calculate the Hamiltonian matrix elements, V_{new} is the new potential calculated from the eigenvectors of the Hamiltonian matrix and $V_{\text{in,next}}$ is the input potential for the next iteration. For the first iteration, V_{in} was comprised of spin-up and spin-down potentials, calculated from the total overlapping free-atom charge densities. The choice of the mixing factor, α, will not affect the final results and α can be chosen between 0 and 1. The larger the α, the fewer are the number of iterations needed. However, a too large α causes the iterations to diverge, i.e. the difference between V_{in} and V_{new} becomes increasingly larger. On the other hand, if an unnecessarily small α is chosen, the number of iterations needed becomes very large and the calculation is very inefficient. The α can be as large as 0.25 for bulk semiconductors with low ionicity and 0.02 for bulk metallic systems within the PSF calculation method. In the present case, due to the very dense energy bands near E_{F}, and the significant charge transfer among the various ions and between spin-up and spin-down states, an unusually small α of 0.002[Note 3] had to be used. A slightly larger α of 0.003 caused the iterations to diverge, especially for the large displacement of Ta ions. This was indeed a very difficult calculation.

The PSF method calculates spin-polarized full charge densities, which include the core charge densities and the corresponding potentials, self-consistently through iterations. The basis set of the PSF method is composed of Bloch sums of muffin-tin orbitals with spherical Hankel and Neumann tailing functions. The linear theory of Andersen [41] is used to solve the Schrödinger equations inside the muffin-tin spheres for the radial component of the muffin-tin orbitals. Since the muffin-tin orbitals change rapidly inside the muffin-tin spheres, a large number of plane waves have to be expanded for calculating the nonspherical and interstitial parts of the Hamiltonian matrix elements. Therefore, the use of pseudofunctions, which are smooth mathematical functions expanded by a minimal number of plane waves, is to improve the efficiency of calculating the nonspherical and interstitial parts of the Hamiltonian matrix elements by the fast Fourier transform (FFT) technique.

For electronic structure calculations in thin films, the PSF method does not use a model with infinitely repeated slabs, as is done in the pseudopotential method. The system used in the PSF method is comprised of the thin film and the vacuum regions on both sides of its surface. However, the PSFs, as well as the nonspherical and interstitial charge densities and potentials in the z coordinate, are expanded in plane waves. Details of the use of three-dimensional plane waves for thin film calculations can be found in [36].

In calculation of the charge densities, the special k-point scheme of Monkhorst and Pack [42], with the number of special k points, $q = 4$, in each direction of the reciprocal vector, is used to approximate the integration over the two-dimensional first Brillouin zone.

[3] The α chosen can be as large as 0.25 for bulk semiconductors with low ionicity. For the PSF calculation method with bulk metallic systems, a typical α is 0.02.

The partial densities of states are calculated by sampling 121 uniform mesh points in the first quadrant of the first Brillouin zone. The muffin-tin radii chosen are 2.60, 2.75, 2.23 and 1.00 a_0 for Sr, Bi, Ta and O, respectively, where a_0 is the Bohr radius. The only constraint in the choice of these muffin-tin radii within the PSF method is that all muffin-tin spheres do not overlap. To limit the number of plane waves used to expand the PSFs, a criterion, $RG_{\max} > n$, where $n = 3$, 5 or 7, respectively, for s, p and d orbitals, is used. The values of n are approximately the first non-zero roots of the spherical Bessel functions and $G_{\max}$ is the largest wavevector in three orthogonal directions. By denoting the three reciprocal basis vectors as b_x, b_y and b_z, the total number of plane waves for PSFs is $(2n_x + 1)\,(2n_y + 1)\,(2n_z + 1)$ with $n_i \sim G_{\max}/b_i$ for $i = x$, y and z. In this study, $G_{\max}$ is chosen such that $RG_{\max} = 13.3$, 14.1 and 11.4, respectively, for Sr, Bi and Ta and $RG_{\max} = 5.1$ for O. With these $G_{\max}s$, $n_x = n_y = 6$ and $n_z = 26$ and the Bloch sums of PSFs are expanded in 8957 plane waves. Since the charge density is the absolute square of the wavefunction, the charge density, as well as the potential, is expanded by $(4n_x + 1)\,(4n_y + 1)\,(4n_z + 1)$ or 65 625 plane waves.

In the current spin-polarized formalism of the PSF method, the sub-matrices for spin-up and spin-down states in the total Hamiltonian matrix are diagonalized separately. Note the off-diagonal sub-matrices, which account for the explicit coupling between spin-up and spin-down states, are ignored. However, coupling between spin-up and spin-down states is implicitly included through the spin-polarized LSDA exchange–correlation potentials of von Barth and Hedin. During the iterations, the spin-up (as well as the spin-down) exchange–correlation potential is calculated as a function of both spin-up and spin-down charge densities. Therefore, in this approach, self-consistent iterations that give the final energy state depend on the spin-polarized starting potential. Consequently, it does not automatically give the final spin-polarized state with the lowest total energy. Thus, the present calculation method cannot predict the thermodynamically most stable spin-polarized state. Here, three starting potentials were considered. One is a paramagnetic starting potential and the other two are spin-polarized. The paramagnetic starting potential is used only for the case when Ta ions sit at the centre of the octahedron. For the two spin-polarized starting potentials, the calculations were done for various off-centre displacements of Ta ions. The first spin-polarized starting potential was obtained by adding a spin-polarized perturbation to the potential of the transition metal Ta ions; Ta ions contain partially filled d shells in the $SrBi_2Ta_2O_{11}$ composition and may be responsible for the unique properties in the system (section 2.1). As will be described later, the first self-consistent iterations using this spin-polarized starting potential yielded a new spin-polarized state (state 1) in which the magnetic moments are located, not at the Ta ion, but predominantly at half of the surface O ions and some at the Sr and O in the Sr–O layer. This initial finding led to the consideration of a second spin-polarized starting potential, in which the spin-polarized perturbation was applied to the potentials of Sr and O in the Sr–O layer and half of the surface O ions. After self-consistent iterations, a final spin-polarized state (state 2), having the largest magnetic moment at the O ions in the central Sr–O plane, was obtained. The relative stability of the paramagnetic state and the spin-polarized states (states 1 and 2) will be determined by comparison of the total energies of these three states (described later).

4. Results and discussion

4.1. Spontaneous electrical polarization

When Ta ions are at the centre of the octahedron, spin-polarized states 1 and 2 are found to have net magnetic moments of 0.83 and 3.37 μ_B per $SrBi_2Ta_2O_{11}$ unit cell, respectively. In the former, the magnetization is due to half of the surface O ions with approximately one unpaired

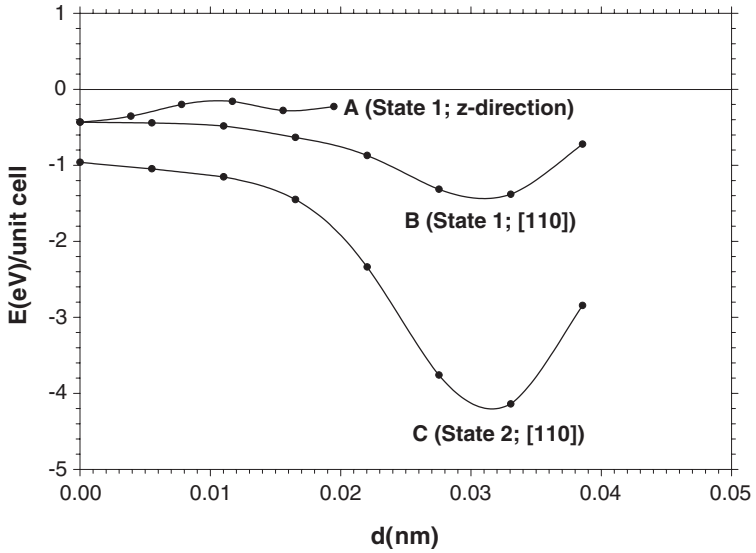

Figure 2. The total energy per unit cell of a $SrBi_2Ta_2O_{11}$ film as a function of the displacement, **d**, of the Ta ion from the centre of the octahedron along the (A) z direction for spin-polarized state 1, (B) [110] for spin-polarized state 1 and (C) [110] for spin-polarized state 2. The zero energy is the total energy per unit cell of the paramagnetic state with $\mathbf{d} = 0$.

2p electron, i.e. O(1) in figure 1, and therefore having a net magnetic moment. In the latter, the magnetization is predominantly due to the O ions in the central Sr–O layer.

Figure 2 illustrates the total potential energy versus the Ta ion displacement, **d**, for spin-polarized states 1 and 2. Curves A and B are for state 1 in which the Ta ions are displaced normal to the surface (z direction) and in the [110] direction, respectively. Curve C is for state 2 in which the Ta ions are displaced in the [110] direction. Curve A indicates that the collective displacement of Ta ions costs energy, so it is unfavourable for all values of **d**. Note that spin-polarized states 1 and 2 at $\mathbf{d} = 0$ have total energies of -0.43 eV/unit cell and -0.96 eV/unit cell relative to that of the paramagnetic state (defined as 0 eV/cell), respectively. The total energy results also show that the state with a larger net magnetic moment (state 2, curve C) is more stable than the one with a smaller moment (state 1, curve B) for all values of **d**. Most importantly, curves B and C exhibit total potential energy minima and their corresponding energy minimum (equilibrium **d**) are -1.0 eV/unit cell (0.031 nm) and -3.1 eV/unit cell (0.032 nm). The total potential energy minimum results from the balance between (a) long-range attractive electrostatic energy (which favours the ferroelectric state) and (b) short-range repulsive strain energy (which favours the paraelectric state) [43]. By symmetry, the same wells exist for $\mathbf{d} \rightarrow -\mathbf{d}$, i.e. the film has double total energy minima for states 1 and 2 and should exhibit spontaneous electrical polarization in the [110] direction. Since the calculated depth of the potential energy well is much larger than the room temperature thermal excitation energy, ferroelectricity will exist at room temperature. Note that the measurement of the in-plane electric polarization in a 1.4 nm film (if it were to be synthesized) by conventional techniques may be difficult. However, the scanning probe technique could be used to measure electric fields (associated with polarization of the film) near the surface.

Now, a question arises as to why a $SrBi_2Ta_2O_{11}$ film spontaneously polarizes in the [110] direction, but not in the z direction. This may be explained on the basis of electrostatics.

The interaction energy between two parallel electric dipoles is given by [44]

$$U = \frac{p^2}{r^3}(1 - 3\cos^2\theta) \tag{1}$$

where p, r and θ are the magnitude of the dipole moments, the distance between dipole moments and the angle between the dipole moments and their adjoining line. Note U is attractive (repulsive) when θ is smaller (larger) than 54.7°. Since the $SrBi_2Ta_2O_{11}$ film contains two octahedral TaO_6 layers per unit cell, there are two TaO_6 octahedrons that are lined up along the z axis. If each octahedron acquires a net dipole moment perpendicular to the film, due to the displacement of Ta ions along the z direction, a given dipole in the lower layer has attractive interactions (since $\theta < 54.7°$) with only five dipoles in the upper layer, whereas it has repulsive interactions with the rest of the numerous dipoles in the film. Thus, the total interaction energy of all dipoles is repulsive and spontaneous electric polarization perpendicular to the film is unfavourable, as shown in figure 2, curve A. When **d** is perpendicular to the film, the relaxation of apex O ions also suppresses the net electric dipole moment of the film. When the collective displacement of Ta ions is in the *ab* plane of the film and in the [110] direction, the dipoles within the TaO_6 octahedra are within the plane. For a given dipole, the total number of dipoles with $\theta < 54.7°$ far outnumber those with $\theta > 54.7°$. Thus, the total interaction energy of all dipoles is attractive and spontaneous electric polarization in the *ab* plane is favourable, as shown in figure 2, curves B and C.

4.2. Electronic structures

One may presuppose that a $SrBi_2Ta_2O_{11}$ film is a wide bandgap, or at least semiconducting, material, but the electronic structures indicate otherwise. The majority spin (↑) and minority spin (↓) band structures of the $SrBi_2Ta_2O_{11}$ film for a spin-polarized state (state 2), with the Ta ions displaced by 0.033 nm in the [110] direction, are shown in figures 3(a) and (b), respectively. Figures 3(c) and (d) show the ↑ and ↓ energy bands near E_F, respectively. These energy bands do not exhibit an energy gap; the film is neither like insulators that have wide energy gaps nor like normal metals that have wide energy bands. The ↑ and ↓ energy bands that straddle E_F are very narrow with widths of 0.4 and 0.3 eV, respectively, which are attributed to the localized nature of Sr and O p orbitals. Most of the intercepts of these energy bands with E_F have negative second derivatives with respect to the wavevector and some are at their inflection point, which corresponds to an infinite effective mass. Note the effective mass of an electron in an energy band is inversely proportional to the curvature of the upward concave band, and due to the complexity of these energy bands an effective mass picture with a positive second derivative is inappropriate. However, based on the narrowness and shape of these energy bands, the material should have a poor conductivity. Figures 3(c) and (d) also show that the spin-down energy bands near E_F are significantly denser than spin-up energy bands, which implies different conduction properties of spin-up and spin-down electrons.

Figure 3 shows that the $SrBi_2Ta_2O_{11}$ film is semi-metallic. Here, semi-metallic means that there are relatively flat bands immediately above E_F. Previously, Hill and Rabe [16] and Hill [22] calculated the band structures of magnetoelectric $BiMnO_3$ in the paramagnetic and ferromagnetic phases and found it to be semi-metallic. Other calculations of the band structure of magnetoelectric $YMnO_3$, in the paramagnetic phase, by Filippetti and Hill [19] and Hill [22] also concur with the results of this $SrBi_2Ta_2O_{11}$ film, i.e. $YMnO_3$ was found to be semi-metallic.

The results in figure 3 may be understood by noting that the electronegativity of Sr (0.85) is much smaller than that of the Ta (1.50) and Bi (2.02) cations in the system [45]. The smaller electronegativity of Sr results in charge transfer or loss of Sr electrons to Bi and Ta ions when

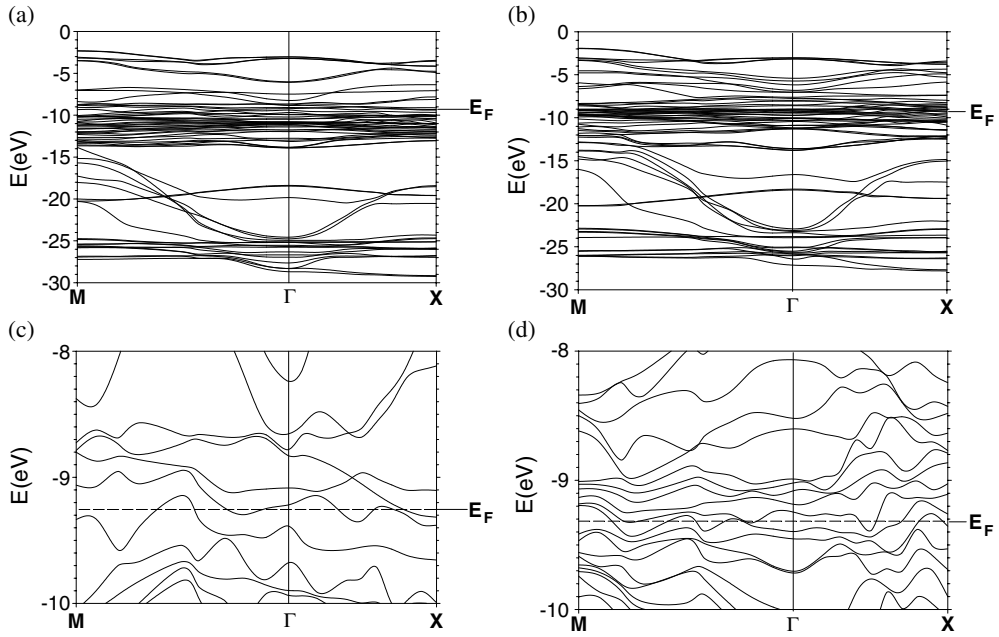

Figure 3. The (a) majority-spin and (b) minority-spin energy bands for the $SrBi_2Ta_2O_{11}$ film. Figures (c) and (d) are plots of the majority-spin and minority-spin energy bands near E_F, respectively. Note Γ, *M* and *X* are the Brillouin zone centre, (π/a) (1, 1) and (π/a) (1, 0), respectively, in K space.

Sr, Ta and Bi oxides are combined to form $SrBi_2Ta_2O_{11}$. The consequent increase in the positive effective charge on Sr further lowers the electrostatic potential at the Sr ion, which effectively lowers the Sr orbital energies. Therefore, the final energy range of the Sr p-derived band and its proximity to E_F is determined by a self-consistent adjustment of the occupation of the Sr p band (figure 4). The calculated Sr p band near E_F can alternatively be envisioned as Sr dopant levels distributed in the energy gap of the Ta and Bi oxides.

Figures 4 and 5 indicate that the bands in the vicinity of E_F predominantly stem from the hybridization between Sr 5p and O 2p orbitals, respectively. Interestingly, the PDOS in magnetoelectric $BiMnO_3$ indicate that the states in the vicinity of E_F stem from hybridization between Bi 6p and Mn 3d orbitals [16, 22]. Likewise, in $YMnO_3$, the states in the vicinity of E_F stem from hybridization between hybridization O 2p and Mn 3d orbitals [19, 22]. Note the major difference between the band structures of bulk SBT [11] (and the $SrBi_2Ta_2O_{11}$ film in this study) to those obtained by Stachiotti *et al* [25] and Peacock and Robertson [26] is the position of the Sr 5p-derived band. Stachiotti *et al* did not observe the Sr 5p-derived band, whereas the Sr 5p-derived band obtained by Peacock and Robertson is higher than E_F by 12 eV. This discrepancy can be resolved by Sr K-edge NEXAFS measurements, as discussed in [11].

Figures 6 and 7 illustrate the calculated PDOS of Bi and Ta, respectively. The 5d (6d) band of Ta (Bi) is located approximately between 15 and 20 eV above E_F. The sharp peaks within the 6s and 6p bands and the symmetry between the ↑ and ↓ PDOS of Bi indicate its localized nature and non-magnetic character. Note the Bi 6p band splits into two sub-bands, located below and above E_F. In contrast, the Ta 6p band spreads over a wide energy range below E_F.

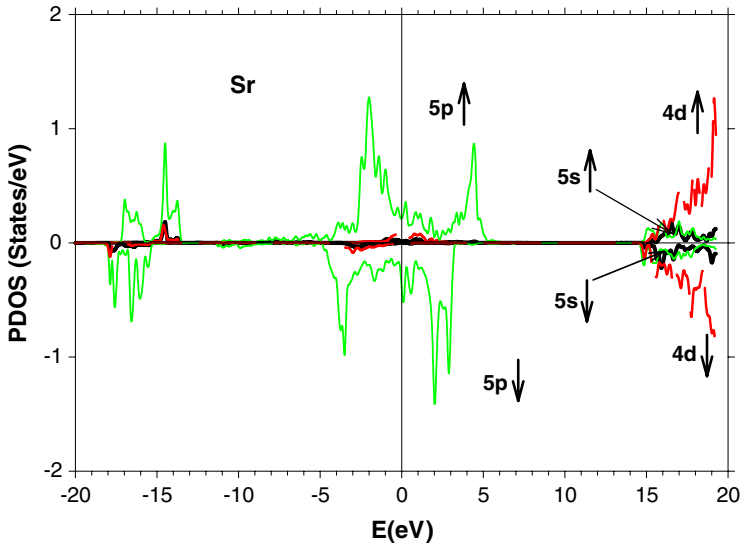

Figure 4. The spin-polarized partial density of Sr-5s, Sr-5p and Sr-4d states with zero energy at E_F.

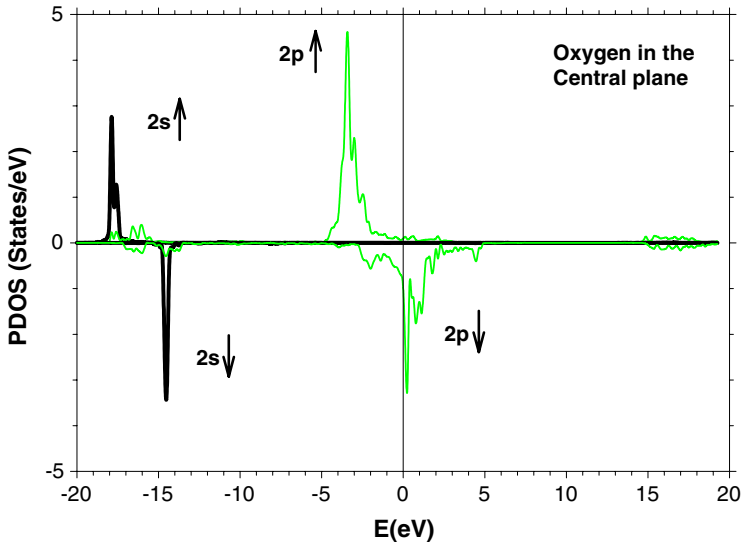

Figure 5. The spin-polarized partial density of O-2s and O-2p states in the Sr–O layer with zero energy at E_F.

4.3. Magnetic properties

The O p PDOS of the O ions in the central Sr–O layer, for a spin-polarized state (state 2), is shown in figure 5. Only the O ions in this central Sr–O layer have highly localized and unpaired 2p orbitals. Note the very sharp O 2p↑ peak at 3.3 eV below E_F, which indicates that the three O 2p↑ orbitals are highly localized and almost fully occupied. Interestingly, the three O 2p↑ electrons in the $SrBi_2Ta_2O_{11}$ film are analogous to the three Mn t_{2g}↑ electrons in manganites and are the origin of the observed magnetic properties in the respective systems [46]. In contrast,

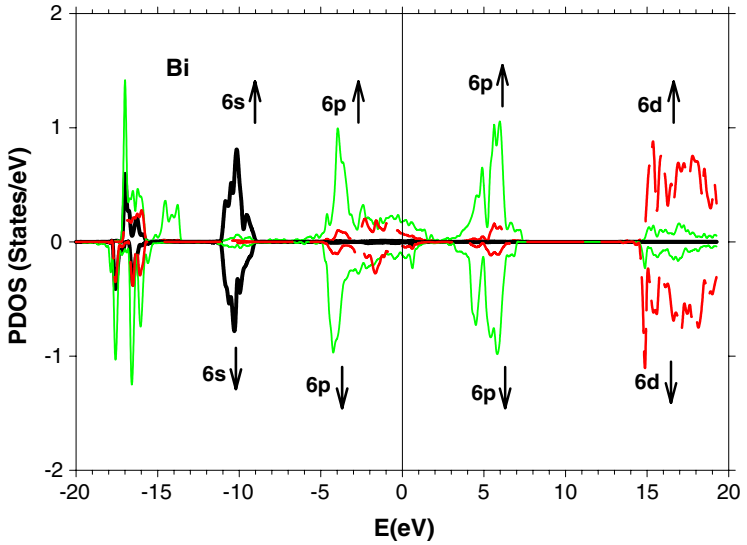

Figure 6. The spin-polarized partial density of Bi-6s, Bi-6p and Bi-6d states. The zero energy is E_F.

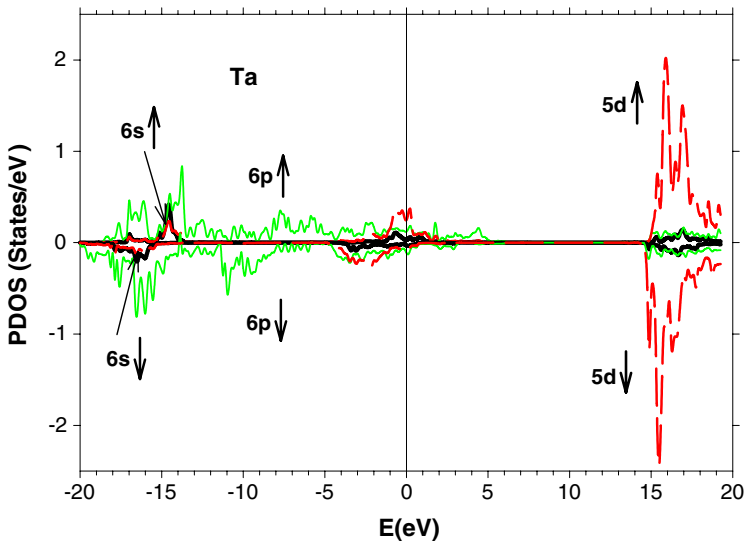

Figure 7. The spin-polarized partial density of Ta-6s, Ta-6p and Ta-5d states. The zero energy is E_F.

the O 2p↓ orbitals are not as localized and a major section of its band is unoccupied because it is predominantly above E_F. Therefore, the difference in occupancy of the ↑ and ↓ bands (which is reflected in the difference in their areas below E_F) gives rise to a net spin or magnetic moment on these O ions in the Sr–O layer.

Figure 4 illustrates the Sr s, p and d ↑ and ↓ PDOS in the central Sr–O layer. Note the shift in the 5p↑ band (with respect to the 5p↓ band) to higher energy can be explained by the Pauli exclusion principle. The spatial confinement of the Sr↑ electrons (due to the surrounding O↑

Table 2. Magnetic moments in Bohr magnetons (μ_B) of all ions.

Surface O(1)ions	0.50 (↑)
Surface O(2)ions	−0.17 (↓)
Apex O ions	−0.30 (↓)
O ions in the Ta layer	0.81 (↑)
O ions in the Sr–O layer	1.32 (↑)
Bi ions	−0.01 (↓)
Ta ions	0.25 (↑)
Sr ions	−0.23 (↓)

electrons) leads to increased kinetic energy and therefore an overall shift in the Sr 5p↑ band to higher energy.

Now the existence of ferromagnetism in the $SrBi_2Ta_2O_{11}$ film merits some comments. Previously, the double exchange model was proposed to explain the coexistence of metallic and ferromagnetic character in doped manganites [46]. In the partially filled $e_g\uparrow$ band of doped manganites, the unoccupied portion mediates the double exchange of highly localized $t_{2g}\uparrow$ spins between adjacent Mn ions. In order to envision the existence of ferromagnetism in the $SrBi_2Ta_2O_{11}$ film, its magnetic coupling mechanism can be correlated with this double exchange model [46]. Here, the unoccupied portion or states of the Sr 5p band (figure 4) above E_F provides a mechanism for the double exchange or hopping of highly localized O 2p↑ spins between adjacent O ions located on both sides of the Sr ion.

If one compares the PDOS to explain the existence of ferromagnetism (in the light of the double exchange model [46]) in the $SrBi_2Ta_2O_{11}$, $BiMnO_3$ [16, 22] and $YMnO_3$ [19, 20, 22] systems, intriguing similarities can be drawn. The hybridization between Sr 5p and O 2p orbitals in $SrBi_2Ta_2O_{11}$, Bi 6p and Mn 3d orbitals in $BiMnO_3$ and O 2p and Mn 3d orbitals in $YMnO_3$ [19, 22] is probably the key to the observance of ferromagnetism in these magnetoelectric materials. The Bi 6p states immediately above E_F in $BiMnO_3$, which are analogous to Sr 5p states in $SrBi_2Ta_2O_{11}$, may well mediate ferromagnetism in $BiMnO_3$. Whereas the O 2p states immediately above E_F in $YMnO_3$ may be the counterpart of Bi 6p states in $BiMnO_3$ and Sr 5p states in $SrBi_2Ta_2O_{11}$.

Table 2 lists the magnetic moments of various ions in the spin-polarized state (state 2) along with their spin direction. The non-magnetic character of Bi is reflected in the low magnitude of its magnetic moment. Clearly, the O ions in the central Sr–O layer have the largest magnetic moment of 1.32 μ_B due to the aforementioned coupling that is mediated by the unoccupied Sr 5p states.

One final thought. When the thickness (i.e. 1.4 nm with two Ta–O octahedral layers in the z direction; figure 1) of the $SrBi_2Ta_2O_{11}$ film increases, the composition of the film will quickly approach that of conventional SBT ($SrBi_2Ta_2O_9$). For example, the composition and thickness of a film with four Ta–O octahedral layers in the z direction will be $Sr_2Ta_2O_{10}$ and ∼2.7 nm (i.e. the lattice constant, c, of a SBT unit cell + 2 times the radius of oxygen ions in oxygen-rich surfaces), respectively. In essence, the O-rich condition is gradually lost as the thickness of the $SrBi_2Ta_2O_{11}$ film is increased. The O-rich condition in $SrBi_2Ta_2O_{11}$ does not mean that the negative and positive charges of the ions in the system are not balanced. Note that $SrBi_2Ta_2O_{11}$ is a molar combination of SrO, Bi_2O_5 and Ta_2O_5, where Bi has an oxidation state of Bi^{5+}. The propensity of the dual oxidation state of the Bi ion (i.e. Bi^{5+} and Bi^{3+}) allows the occurrence of highly localized and unpaired O p orbitals that promote ferromagnetic coupling via the Sr ion. Without this driving force for ferromagnetic coupling, unpaired and highly localized O 2p orbitals may not occur. For thicker films, the localization

as well as the non-bonding condition of O 2p states, which is essential for magnetism, will no longer exist. Thus, ferromagnetism may only exist in nm-thick films.

5. Conclusion

Due to the need for novel multifunctional materials in nanoscience and nanotechnology, spin-polarized first-principles calculations were carried out on a $SrBi_2Ta_2O_9$ or SBT-derived film (of nm dimensions) to determine its potential for exhibiting unique multi-ferroic properties. The 1.4 nm film, of composition $SrBi_2Ta_2O_{11}$, is a sub-cell of conventional SBT and is comprised of a bottom $(BiO_2)^{1+}$ layer, a central $(SrTa_2O_7)^{2-}$ layer and a top $(BiO_2)^{1+}$ layer. The calculations included the electronic structure and the total energy and it was found that the $SrBi_2Ta_2O_{11}$ film is magnetoelectric, i.e. it simultaneously exhibits ferroelectric and ferromagnetic characteristics.

The majority spin (↑) and minority spin (↓) band structures of the $SrBi_2Ta_2O_{11}$ film, with Ta ions collectively displaced in the *ab* plane and in the [110] direction, indicate its semi-metallic nature. The effective masses of electrons in these bands are large and the electrons do not have a high mobility. The calculated results of the total potential energy as a function of Ta ion displacements, in the *ab* plane and in the [110] direction, show a double potential energy well. This reflects the spontaneous polarization or ferroelectric behaviour in the $SrBi_2Ta_2O_{11}$ film. From the features in the calculated PDOS of O and Sr, the double exchange model is used to explain the ferromagnetic behaviour in the $SrBi_2Ta_2O_{11}$ film. The unoccupied states of the Sr 5p band above E_F provides a mechanism for the double exchange of highly localized O 2p↑ spins between adjacent O ions located on both sides of the Sr ion in the Sr–O layer. In contrast to other magnetoelectric materials, such as $BiMnO_3$, $YMnO_3$ and $BiFeO_3$, the d electrons of the transition metal (Ta in this case) do not play a significant role in enforcing the magnetic behaviour in the $SrBi_2Ta_2O_{11}$ film.

Due the strong potential for the observance of additional and unique properties (e.g. piezoelectric, optical, dielectric, pyroelectric, etc) in $SrBi_2Ta_2O_{11}$, the fabrication of 1.4 nm films is immediately warranted.

Acknowledgments

MHT and YHT wish to thank the National Science Council of Republic of China for their support (contract no NSC 91-2112-M-110-013). SKD appreciates the financial support from NSF (grant number ECS 0000121) and DARPA (grant number 15428) for novel dielectric materials and device research at Arizona State University.

References

[1] Scott J F and Paz de Araujo C A 1989 *Science* **246** 1400
[2] Evans J T and Womack R 1988 *IEEE J. Solid-State Circuits* **23** 1171
[3] Rae A D, Thompson J G and Withers R L 1992 *Acta Crystallogr.* B **48** 418
[4] Kato K, Zheng C, Finder J and Dey S K 1998 *Am. Ceram. Soc.* **81** 1869
[5] Dey S K and Zuleeg R 1990 *Ferroelectrics* **108** 37
[6] Dey S K 1996 *Mater. Res. Soc. Bull.* **21** 44
[7] Barz R, Amrhein F, Shin Y and Dey S K 1998 *Integr. Ferroelectr.* **22** 65
[8] Larsen P K, Dormans G J M, Taylor D and Van Veldhoven P J 1994 *J. Appl. Phys.* **76** 2405
[9] Mihara T, Yoshimori H, Watanabe H and Paz de Araujo C A 1995 *Japan. J. Appl. Phys.* **34** 5233
[10] Paz de Araujo C A, Cuchiaro J D, McMillan L D, Scott M C and Scott J F 1995 *Nature* **374** 627
[11] Tsai M-H and Dey S K 2000 *IEEE Trans. Ultrason. Ferroelectr. Freq. Control* **47** 929

[12] Lide D R (ed) 1992 *CRC Handbook of Chemistry and Physics* 73rd edn (Boca Raton, FL: Chemical Rubber Company)
[13] Scott J F 1979 Phase transitions in $BaMnF_4$ *Rep, Prog. Phys.* **42** 1055
[14] Scott J F 1986 Statics and dynamics of incommensurate $BaMnF_4$ *Dielectric Properties of Incommensurate Phases* ed R Blinc and A P Levanyuk (Amsterdam: North-Holland) p 283
[15] Spaldin N A 2002 *15th Int. Symp. on Integrated Ferroelectrics (Colorado Springs, CO, USA, March 2002)* p 320 (Book of abstracts) at press
[16] Hill N A and Rabe K M 1999 *Phys. Rev.* B **59** 8759
[17] Seshadri R and Hill N A 2001 *Chem. Mater.* **13** 2892
[18] Huang Z J, Cao Y, Sun Y Y, Xue Y Y and Chu C W 1997 *Phys. Rev.* B **56** 2623
[19] Filippetti A and Hill N A 2001 unpublished manuscript
[20] Wang J, Neaton J B, Zheng H, Nagarajan V, Ogale S B, Liu B, Viehland D, Vaithyanathan V, Schlom D G, Waghmare U V, Spaldin N A, Rabe K M, Wuttig M and Ramesh R 2003 *Science* **299** 1719
[21] Also see Freeman A J and Schmmidt H (ed) 1975 *Magnetoelectric Interaction Phenomena in Crystals* (New York: Gordon and Breach)
1994 *Proc. 2nd Int. Conf. on Magnetoelectrics (Ascona, Switzerland) Ferroelectrics* **161** (special volume)
[22] Hill N A 2002 *Annu. Rev. Mater. Res.* **32** 1–37
[23] Robertson J, Chen C W, Warren W L and Gutleben C D 1996 *Appl. Phys. Lett.* **69** 1704
[24] Robertson J and Chen C W 1999 *Appl. Phys. Lett.* **74** 1168
[25] Stachiotti M G, Rodriguez C O, Ambrosch-Draxl C and Christensen N E 2000 *Phys. Rev.* B **61** 14434
[26] Peacock P W and Robertson J 2002 *J. Appl. Phys.* **92** 4712
[27] Hartmann A J, Lamb R N, Scott J F and Gutleben C D 1997 *Integr. Ferroelectr.* **18** 101
[28] Hartmann A J and Scott J F 1997 *Ferroelectr. Lett.* **23** 75
[29] Baudry L and Tournier J 2001 *J. Appl. Phys.* **90** 1442
[30] Junquera J and Ghosez P 2003 *Nature* **422** 506
[31] Zembilgotov A G, Pertsev N A, Kohlstedt H and Waser R 2002 *J. Appl. Phys.* **91** 2247
[32] Shaw T M, Trolier-McKinstry S and McIntyre P C 2000 *Annu. Rev. Mater. Sci.* **30** 263
[33] Ganpule C S, Stanishevsky A, Su Q, Aggarwal S, Melngailis J, Williams E and Ramesh R 1999 *Appl. Phys. Lett.* **75** 409
[34] Mehta R R, Silverman B D and Jacobs J T 1973 *J. Appl. Phys.* **44** 3379
[35] Wurfel P and Batra I P 1974 *Ferroelectrics* **7** 261
[36] Watanabe Y 1998 *Phys. Rev.* B **57** 789
[37] Wurfel P, Batra I P and Jacobs J T 1973 *Phys. Rev. Lett.* **24** 1218
[38] Batra I P and Silverman B D 1972 *Solid State Commun.* **11** 291
[39] Kasowski R V, Tsai M-H, Rhodin T N and Chambliss D D 1986 *Phys. Rev.* B **34** 2656
[40] von Barth U and Hedin L 1972 *J. Phys. C: Solid State Phys.* **5** 1629
[41] Andersen O K 1976 *Phys. Rev.* B **12** 3060
[42] Monkhorst H J and Pack J D 1976 *Phys. Rev.* B **13** 5188
[43] Cohen R E 1992 *Nature* **358** 136
[44] Jackson J D 1975 *Classical Electrodynamics* 2nd edn (New York: Wiley)
[45] *Table of Periodic Properties of the Elements* 1980 (Skokie, IL: Sargent-Welch Scientific Company)
[46] Tokura Y (ed) 2000 *Colossal Magnetoresistive Oxides* (The Netherlands: Gordon and Breach)
Dagotto E, Hottta T and Moreo A 2001 *Phys. Rep.* **344** 1